machines

MDPI

Article

Multi-Objective Optimization of Machinability and Energy Consumption of Cast Iron Depending on Cooling Rate

Burak Öztürk [1] and Fuat Kara [2,*]

[1] Department of Metallurgical and Materials Engineering, Engineering Faculty, Bilecik Şeyh Edebali University, 11230 Bilecik, Türkiye; burak.ozturk@bilecik.edu.tr
[2] Department of Mechanical Engineering, Engineering Faculty, Düzce University, 81620 Düzce, Türkiye
* Correspondence: fuatkara@duzce.edu.tr

Abstract: Cooling rates in cast iron significantly impact its microstructure, leading to bainitic transformation instead of ferritic structures, resulting in microstructures with higher pearlite content and even cementite formation. Consequently, this transformation causes hardness values to vary between 160 and 320 HB, directly affecting the material's machinability. Energy efficiency has become a critical focus in sustainable production techniques and cost-effective machining processes. This variation directly influences machinability, with higher hardness generally improving surface quality. Energy efficiency in machining is crucial for sustainable production, and Specific Cutting Energy Consumption (SCEC) has become a key metric in evaluating machinability. Using genetic algorithms (GA) and Response Surface Methodology (RSM), this study optimized machining parameters for energy consumption and surface finish. GA results indicated that a cutting speed of 200 m/min and a feed rate of 0.15 mm/rev minimized surface roughness to 1.359 Ra while reducing Specific Energy Consumption (SEC) from 3.25 to 2.83 Wh/mL. The lowest surface roughness (1.0 µm) was observed at a hardness of 320 HB, with the same cutting parameters. RSM analysis identified optimal parameters as a cutting speed of 150–200 m/min, a feed rate of 0.2 mm/rev, and a hardness of 220–245 HB, balancing energy efficiency and surface quality. ANOVA showed that cutting speed and feed rate contributed to 30% of the surface roughness variability and 45% of the energy consumption variability.

Keywords: SEC; coolin rate; RSM; GA

Academic Editor: Angelos P. Markopoulos

Received: 9 December 2024
Revised: 16 January 2025
Accepted: 21 January 2025
Published: 23 January 2025

Citation: Öztürk, B.; Kara, F. Multi-Objective Optimization of Machinability and Energy Consumption of Cast Iron Depending on Cooling Rate. *Machines* **2025**, *13*, 84. https://doi.org/10.3390/machines13020084

1. Introduction

Cast irons are a significant group of materials widely used in the industry [1]. The mechanical properties of these materials can vary significantly depending on production conditions, particularly cooling rate and microstructure. The cooling rate directly affects the microstructure of cast iron, determining crucial properties such as hardness and machinability [2]. The cooling rate of cast iron varies depending on several factors, such as the material's wall thickness, volume, and environmental conditions. Environmental factors, such as the moisture content of the sand or ambient temperatures, can influence the cooling rate of cast iron, thereby altering its microstructure. However, the primary focus here is not on the changes in chemical composition but rather on the effect of the solidification rate during casting on the material's properties [3,4]. In a study, the damage mechanisms of nodular cast iron under tensile stress were analyzed, focusing on two key phenomena: internal destruction of graphite nodules and debonding at the graphite/matrix interface. Microscopic observations revealed that the paths of internal cracks in graphite nodules passed through regions of weakened cohesion, while the graphite/matrix debonding was

influenced by the phase characteristics of the metal matrix and the proximity to the main crack surface. Additionally, the study highlighted that in alloys with ferritic and ausferritic matrices, a shifted layer of graphene plates formed before debonding, whereas in polyphase matrices, interactions with cementite lamellae and austenite plates delayed the debonding process [5].

There are some studies in the literature examining the cooling rates and microstructure changes of cast irons. The effects of varying cooling rates during the austempering process on the microstructure and mechanical properties of ferritic spheroidal cast iron have been investigated. The study revealed the relationship between hardness and microstructural changes concerning changes in cooling temperatures, directly impacting machinability properties [6]. These findings are supported by studies examining the effects of casting temperatures and filling rates on the fluidity properties of lamellar graphite cast iron [7]. When combined with research on the deformation parameters of GGG 40 spheroidal cast iron under low temperatures and slow deformation rates, these findings demonstrate how deformation temperatures and rates promote dynamic recrystallization, improving mechanical properties through changes in graphite morphology [8]. A study examined the effects of heat treatment on the microstructure, mechanical, and tribological properties of unalloyed and alloyed ductile iron, revealing improved tensile strength, hardness, and wear resistance with varying austenitizing temperatures. The process produced ferritic and martensitic structures and demonstrated a dual wear mechanism of abrasion and oxidation under tribological testing [9]. Research on the microstructure and mechanical properties of explosively bonded 304 stainless steel and CK45 carbon steel after heat treatment has shown how heat treatment improves microstructural changes at the interfaces of bonded materials and enhances their mechanical properties [10]. This study is complemented by research on the microstructure and mechanical properties of Al/Fe bimetallic castings after heat treatment, detailing how heat treatment promotes the formation of intermetallic phases at the interfaces of materials and examines their effects on mechanical performance [11]. However, the literature on how the microstructures obtained through cooling rates impact the machinability of cast iron remains limited. Most studies have analyzed the machinability of cast irons based on energy consumption data, which has been noted as a quick and straightforward evaluation method. Nonetheless, more in-depth research is needed on how machinability changes with cooling rates in cast iron. This gap stems from the limited number of studies examining the relationship between structures formed under different cooling rates and their machinability.

These studies underscore the transformative impact of heat treatment on the microstructural and mechanical properties of spheroidal cast materials, emphasizing their vital role in optimizing material selection and engineering processes. Moreover, existing literature predominantly centers on overarching topics, such as energy consumption and efficiency, leaving a gap in understanding the nuanced relationship between microstructural changes and machinability. Additionally, the literature indicates that most studies focus on broader topics, such as energy consumption and efficiency [12–15]. Therefore, new approaches should be developed to deeply examine the relationship between surface roughness and machinability of cast irons. Research on the machinability and energy consumption of spheroidal cast iron indicates that despite its superior mechanical properties, this material presents challenges during machining, necessitating optimization of energy consumption. Ataş et al. (2023) optimized the process parameters for milling austempered spheroidal cast iron (GGG70) using the bee algorithm. They conducted experiments with different cutting fluid types, cutting speeds, and depths of cut using minimum quantity lubrication (MQL) [12]. Düzce and Samtaş (2021) analyzed the effects of cutting parameters on cutting temperature and their optimization during the milling of GG25 cast iron. They

performed experiments using cutting tools with different coatings, cutting speeds, feed rates, and cutting depths for surface milling operations [13]. A study explored the use of magnesium alloy in the Tundish + Cored Wire injection method to produce vermicular graphite cast irons with a pearlitic-ferritic matrix (~25% ferrite). The findings show that adjusting the cored wire length based on sulfur content and melt weight ensures high-quality vermicular graphite irons under industrial conditions [14]. Kai Ma and colleagues developed the Cutting Distance with Equal Energy (CDEE) method to evaluate machinability effectively. Using the Drop Hammer Orthogonal Cutting (DHOC) test machine driven by gravitational potential energy, they simplified the process without requiring expensive equipment [15]. Recent research on the machinability of cast irons has primarily focused on the relationship between material types and energy consumption during machining. These studies have provided faster and more efficient evaluation methods for assessing the machinability of cast irons, which are particularly beneficial for industrial production processes. However, the relationship between the structures obtained through different cooling rates and their machinability warrants more detailed examination [16].

Furthermore, in recent years, energy consumption has become a significant phenomenon in assessing machinability [17–19]. One study explored the milling of 6061 aluminum alloy, focusing on calculating and predicting surface roughness and energy consumption [17]. It provided detailed insights into how machining parameters influence energy use and surface quality, offering practical guidance for optimizing both in engineering applications. Similarly, another investigation used the Taguchi method to optimize surface roughness and examined energy consumption during the milling of spheroidal graphite cast iron [18]. This work highlighted the role of machining parameters in energy use and suggested experimental strategies to enhance surface quality. Another research effort looked into the relationship between energy consumption and surface roughness in slot milling operations, specifically considering the impact of *X*-axis and spindle servo motors [19].

Studies are carried out on the optimization of machining processes and machinability using different optimization methods. Thus, both optimizations are made in the manufacturing process, the number of experiments is reduced, and linear results are obtained. Cryogenic cooling in high-feed turning has shown remarkable potential for enhancing the machinability of Haynes 263 and Inconel 718 superalloys by reducing cutting forces, improving surface finish, and minimizing tool wear, offering a more efficient alternative to traditional methods [20]. For threading austempered ductile iron (ADI), advanced PVD coatings such as AlTiSiN, particularly when pre-treated with drag grinding, significantly enhance tool durability and lower cutting torque, ensuring superior threading quality [21]. The use of ceramic tools for machining ADI is also promising, provided that cutting conditions are optimized to reduce wear. This approach offers efficient material removal with acceptable surface integrity and manageable wear mechanisms [22]. In high-speed milling, spray-applied cutting fluids, also known as Minimum Quantity Lubrication (MQL), effectively reduce thermal effects and tool degradation while improving finish quality, making it a sustainable alternative for precision machining [23]. This study examines the machinability of cast iron products with varying cooling rates, which consequently lead to changes in their mechanical and metallurgical properties, using optimization techniques. Through the use of paired graphs, the impact ratios of results are analyzed and compared using RSM (Response Surface Methodology) and GA (Genetic Algorithm) techniques. This approach aims to identify the optimal levels for chip-removal manufacturing processes.

2. Materials and Methods

2.1. Material Properties and Energy Consumption in Machining

This study aims to differentiate itself from the literature by examining the structures obtained under different cooling rates and their effects on machinability. In this regard, material properties have been optimized using modern methods such as genetic algorithms. Genetic algorithms enable the determination of optimal material properties by analyzing various parameters. Consequently, the optimum machinability conditions for cast irons will be compared with parameters such as surface roughness and hardness, and more efficient production methods will be developed in light of these comparisons.

Surface roughness is directly related to the hardness of the material, offering significant insights into machinability. The machinability properties of cast iron samples produced under different cooling rates with hardness values ranging from 160–320 Brinell will be analyzed and optimized with time-varying specific energy consumption functions. This study will significantly contribute to more accurately analyzing the machinability of cast irons and developing more efficient solutions for industrial production processes. As the flow chart is given in Figure 1, this experiment was completed in a total of 5 steps, and the materials and methods used for each step are explained, respectively.

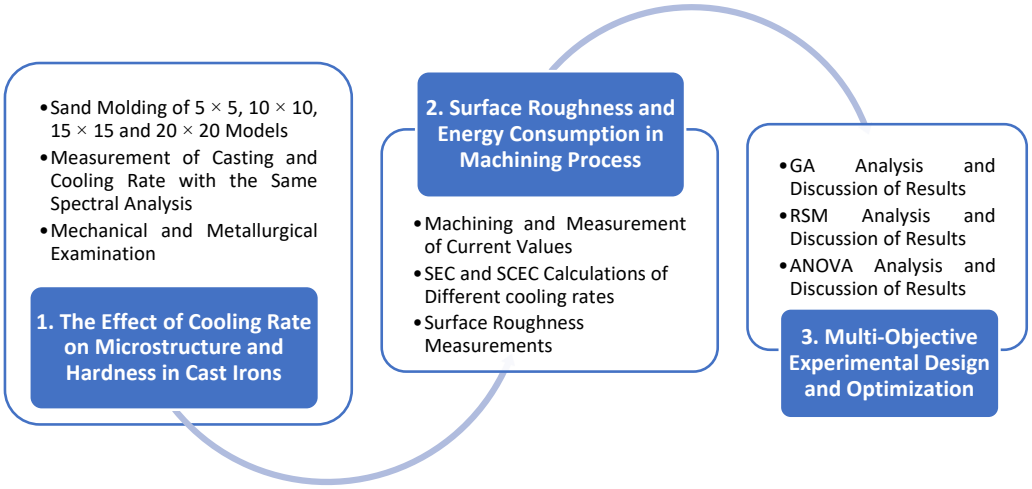

Figure 1. Experimental flow chart.

In order to obtain cast iron samples with 4 different hardness and microstructure values, samples with thicknesses of 5 × 5, 10 × 10, 15 × 15 and 20 × 20 were produced. Two percent moisture sand was prepared for molding. The molding process was performed in mechanical presses; each model length was 100 mm. Temperature changes from the casting follow-way were measured with the help of a laser thermometer, and this change was turned into a graph. During casting, casting was carried out from GGG 42 ductile iron material according to the spectral analysis results in Table 1. Thus, microstructure, workability, and mechanical and metallurgical properties depending on different cooling rates could be examined.

The experimental design was based on three main input parameters: hardness, cutting speed, and feed rate. Hardness values ranged from 170 HB to 320 HB, cutting speeds from 100 m/min to 200 m/min, and feed rates from 0.15 mm/rev to 0.25 mm/rev. These parameters were randomly selected during population creation, with each individual representing a solution candidate (Table 2). The outputs were determined as surface roughness, SEC, and SCEC.

Table 1. Spectral analysis results of the test substance.

Element	Analysis 1	Analysis 2	Analysis 3	Average
Fe	93.300	93.200	93.300	93.300
C	3.620	3.600	3.530	3.580
Si	2.620	2.650	2.650	2.640
Mn	0.146	0.143	0.143	0.144
P	0.030	0.033	0.034	0.032
S	0.016	0.015	0.015	0.015
Cr	0.028	0.028	0.027	0.027
Mo	0.004	0.005	0.004	0.005
Ni	0.017	0.020	0.017	0.018
Al	0.008	0.007	0.007	0.007
Co	0.002	0.001	0.002	0.002
Cu	0.023	0.018	0.019	0.020
Mg	0.049	0.050	0.043	0.047
Nb	0.002	0.002	0.002	0.002
Ti	0.015	0.017	0.016	0.016
V	0.006	0.007	0.006	0.006
Pb	0.005	0.005	0.005	0.005
Sn	0.009	0.010	0.011	0.010
B	0.001	0.001	0.001	0.001
Ca	0.002	0.005	0.005	0.003
Ce	0.028	0.032	0.028	0.029
Zr	0.006	0.008	0.007	0.007
Zn	0.007	0.008	0.007	0.007
Bi	0.005	0.008	0.009	0.007
As	<0.0030	<0.0047	<0.0056	0.0043
La	0.011	0.0109	0.0091	0.0103
Sb	<0.0050	<0.0050	<0.0050	0.005
Se	<0.0050	0.0058	0.0119	0.0071

Table 2. Experimental design.

Experiment Number	Hardness (HB)	Cutting Speed (m/min)	Feed Rate (mm/rev)
1	170	100	0.15
2	170	100	0.20
3	170	100	0.25
4	170	150	0.15
5	170	150	0.20
6	170	150	0.25
7	170	200	0.15
8	170	200	0.20
9	170	200	0.25
10	230	100	0.15
11	230	100	0.20
12	230	100	0.25
13	230	150	0.15
14	230	150	0.20
15	230	150	0.25
16	230	200	0.15
17	230	200	0.20
18	230	200	0.25
19	280	100	0.15
20	280	100	0.20
21	280	100	0.25
22	280	150	0.15

Table 2. *Cont.*

Experiment Number	Hardness (HB)	Cutting Speed (m/min)	Feed Rate (mm/rev)
23	280	150	0.20
24	280	150	0.25
25	280	200	0.15
26	280	200	0.20
27	280	200	0.25
28	320	100	0.15
29	320	100	0.20
30	320	100	0.25
31	320	150	0.15
32	320	150	0.20
33	320	150	0.25
34	320	200	0.15
35	320	200	0.20
36	320	200	0.25

The fitness function was designed to minimize the combined total of these outputs. For this purpose, surface roughness was calculated based on hardness and feed rate, SEC represented energy consumption related to cutting speed, and SCEC highlighted the effect of feed rate and hardness on energy efficiency. These three metrics were evaluated to achieve the best results during the optimization process.

The Microcut CNC vertical machining center, capable of operating at speeds up to 15,000 rpm, was used for high-precision operations. In this study, the workpiece was clamped in a precision vice and machined using the slot milling method. The cutting tool was an 8 mm diameter, three-flute TaeguTec end mill operated with 50% side-step and 2 mm depth of cut. It is a tool with AlTiCrN coating, a 45-degree Flute Helix Angle, and 3 cutting edges. This tool exhibited excellent performance for slotting, profiling, and precision surface finishing operations. Current measurements were performed using a current transformer connected to the machine. The current transformer measured the values of each phase separately, transmitted them to a display, and recorded the data in real-time. The current indices, measured in amperes, provided reliable data for evaluating energy consumption and process stability.

Energy Consumption (E) has become an essential evaluation criterion in machining processes in recent years. While it is typically calculated using the basic motor power equation, it has been simplified and presented in this article as a time-dependent equation. It calculates the total energy consumed by a three-phase motor within the time interval. Electrical energy is derived through the integration of instantaneous current, voltage, and power factor multipliers. The coefficient 0.658 in the equation is derived from the product of voltage and power factor. This energy is expressed in kWh or J. The formula for energy consumption is given in Equation (1).

$$E = 0.658. \int_{T_1}^{T_2} I(t)dt \quad (1)$$

Material Removal Volume (mm^3) can also be calculated considering time-dependent variations in parameters like feed rate, depth of cut, tool diameter, and spindle speed. This volume is determined using an integral approach for time-varying conditions and is also expressed in mm^3 or mL. The formula for material removal volume (mm^3) is given in Equation (2).

$$V_{removed} = \int_{T_1}^{T_2} f(t).\, a_p\,(t).\, \pi\,.\, D(t).\, n(t)dt \quad (2)$$

Specific Energy Consumption (SEC) illustrates the relationship between energy consumed and the volume of material removed. Assuming a constant current (A), it applies to cases where material removal parameters remain constant. SEC is typically expressed in or. The formula for SEC is given in Equation (3).

$$SEC = \frac{I}{2.067.f.a_p\ .D.n} \tag{3}$$

Specific Cutting Energy Consumption (SEC) also explains the relationship between energy consumption and time-dependent variations. The formula for SEC is given in Equation (4).

$$\mathrm{SCEC} = \frac{[\mathrm{I_{total}} - \mathrm{I_{idle}}]}{2.067.\mathrm{f.a_p.D.n}} \tag{4}$$

The machinability properties of different microstructures that occur depending on the cooling rate changes have been investigated in this article according to the determined experimental design parameter levels. The calculations were made to find the amount of energy required to remove 1 mL of material during cutting and provide information about how much the general machinability properties of a material can change. The properties of machinability, depending on different material removal parameters, have been examined in this research by evaluating the specific cutting and total energy consumption values. In addition, a reference source has been created to explore the machinability properties of different materials with the help of formulas given in the simplest form.

Surface roughness measurements were conducted in the laboratory of Bilecik Şeyh Edebali University using the Mitutoyo Surftest SJ-201P roughness tester. The Mitutoyo Surftest SJ-201P is manufactured by Mitutoyo Corporation, headquartered in Kawasaki, Kanagawa, Japan. His device offered high precision in surface profile analysis, providing critical data for evaluating manufacturing processes. Surface roughness measurements were conducted by selecting three sections from the test sample: the beginning, middle, and end. Each section was measured with three test repetitions. The average surface roughness (Ra) was then calculated based on the results obtained for each sample.

2.2. Multi-Objective Optimization

Genetic algorithms (GAs) are methods inspired by biological evolutionary processes that provide solutions to complex optimization and search problems. These algorithms mimic natural selection and genetic mechanisms to effectively search large solution spaces. In the late 1960s, American computer scientist John Holland developed the foundational principles of genetic algorithms. In his 1975 book *Adaptation in Natural and Artificial Systems*, he detailed the theoretical basis of these methods [24]. Holland's student, David E. Goldberg, applied genetic algorithms in his 1983 doctoral dissertation to optimize and control gas pipelines. His 1989 book *Genetic Algorithms in Search, Optimization, and Machine Learning* popularized genetic algorithms among a wider audience [25]. Today, genetic algorithms are widely used in technology-focused countries such as the United States, Japan, Germany, and the United Kingdom, particularly in fields like engineering, artificial intelligence, and bioinformatics [26–29].

In this study, the genetic algorithm method was used to optimize the effects of input parameters on outputs, such as surface roughness, specific energy consumption (SEC), and specific cutting energy consumption (SCEC). The feasibility and accuracy of the study were ensured using the Python programming language. The DEAP library was selected as the primary tool for efficiently implementing genetic algorithms. DEAP simplifies all stages of genetic algorithms, including population creation, fitness function evaluation, selection,

crossover, and mutation. Additionally, the NumPy library was utilized for data processing and analytical calculations.

The stages of the genetic algorithm were defined as follows: random creation of the initial population, selection of suitable individuals based on fitness values, combination of genetic material through crossover, and ensuring population diversity through mutation. At the end of each generation, fitness values were evaluated, and the algorithm was terminated once a predefined number of iterations were reached or when the results were sufficiently stabilized. The results obtained throughout the study demonstrated that genetic algorithms are an effective tool for finding the best combinations in large solution spaces. A Python code was used to solve the set of experiments using a ge netic algorithm. The code uses the DEAP library and is structured to optimize the inputs (hardness, cutting speed and feed rate) for the outputs (surface roughness, SEC and SCEC).

In this study, an RSM (Response Surface Methodology) analysis was performed, which differed from the genetic algorithm. In this way, the results of both methods and the three-dimensional surface plots created were compared. These surface plots were generated using specific functions in each study. In genetic algorithms, the fitness function is typically used. This function, which is one of the core components of genetic algorithms, evaluates how well each individual performs and is defined based on the optimization target. On the other hand, RSM analysis commonly utilizes second-degree polynomial functions. These functions are created based on data obtained through experimental design and aim to understand the relationships between dependent and independent variables. These two calculation methods were compared based on the generated surface plots and energy consumption results. It should be noted that in genetic algorithms, the graphs of pairwise combinations are analyzed, whereas, in RSM analysis, a surface map for two selected parameters is created and evaluated in three dimensions. Therefore, these two methods were brought together to compare their advantages and disadvantages and to evaluate which performs better under specific conditions. RSM (Response Surface Methodology) is a statistical technique used in experimental design and optimization processes. It was first developed in the 1950s by George E. P. Box and K. B. Wilson. This method aims to model and analyze results obtained from experimental data to understand and optimize the relationships between dependent and independent variables [30,31].

In engineering, RSM is widely used, particularly in the optimization of manufacturing processes, determination of material properties, and analysis of energy consumption. Additionally, RSM analyses are applied in areas such as machining, chemical engineering, biomedical research, and quality control studies. This method is preferred for its ability to provide effective results in complex processes, reduce costs, improve production quality, and create more efficient workflows [32,33]. In this study, ANOVA analysis was conducted using the Minitab 19 software for all experimental design parameters, with models and outputs considered as response variables. The percentage effect ratios were also examined.

3. Results and Discussion

3.1. The Effect of Cooling Rate on Microstructure and Hardness in Cast Irons

After preparing the casting sand, two molds of each model were created, resulting in a total of four different models. All castings were made using the same crucible. Cooling rates after casting were measured using a laser meter. The microstructure of cast iron is a critical factor in determining its mechanical properties. The relationship between cooling rate, hardness, and microstructure has a direct impact on the machinability and usability of cast iron. Components such as ferrite, pearlite, and cementite, which constitute the microstructure, vary based on parameters like cooling rate and cooling time (e.g., the cooling duration shown in Figure 2). These variations significantly influence the material's

hardness values. In this context, the cooling rates and hardness values of the four models clearly illustrate the transformation processes in the microstructure and their effects on the material's properties.

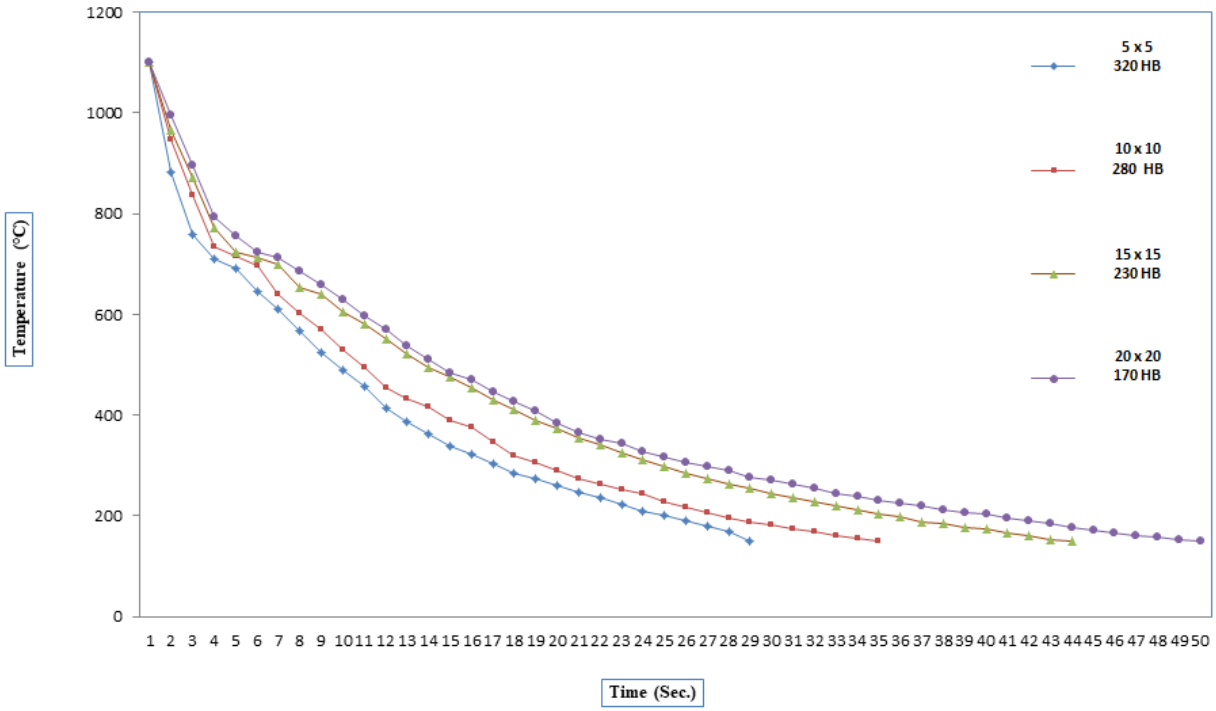

Figure 2. Cooling rate curves for materials with different volumes.

Figure 3 illustrates the relationship between microstructure variations, hardness, and cooling rate for materials derived from the same batch and furnace under four distinct models: The first model, composed entirely of cementite, showed the highest hardness value (320 HB) and the fastest cooling rates: 2.85 °C/s between 1100–800 °C and 0.54 °C/s between 1100–150 °C. While cementite substantially increases hardness, it also brings brittleness, highlighting the trade-off between strength and toughness. The data confirm a strong link between higher cooling rates and increased hardness. The second model, containing 70% pearlite and 30% ferrite, had cooling rates of 2.20 °C/s (1100–800 °C) and 0.41 °C/s (1100–150 °C), with a hardness of 280 HB. The addition of ferrite reduced hardness and slowed the cooling process. While ferrite enhanced flexibility, the increased pearlite content contributed to a more uniform microstructure. In the third model, with 30% pearlite and 70% ferrite, the cooling rates dropped further to 1.96 °C/s (1100–800 °C) and 0.34 °C/s (1100–150 °C), while the hardness decreased to 230 HB. Ferrite's ability to absorb heat extended the cooling time, leading to a softer and more flexible structure. The final model, consisting entirely of ferrite, exhibited the slowest cooling rates: 1.66 °C/s (1100–800 °C) and 0.30 °C/s (1100–150 °C), with the lowest hardness value (170 HB). Increasing the ferrite content maximized flexibility.

The microstructural images in Figure 4 visually depict the changes in material cooling rate for the four models, correlating with their respective hardness and cooling rate values. The 100% cementite model displays a densely packed structure with minimal porosity, which aligns with its high hardness (320 HB) and rapid cooling rates. As the ferrite content increases across the models, the microstructure becomes more open and less dense, reflecting enhanced flexibility and reduced hardness. The 70% pearlite and 30% ferrite model shows a balanced microstructure with intermediate cooling rates and hardness (280 HB). Meanwhile, the 30% pearlite and 70% ferrite model exhibits a more ferritic

structure with reduced hardness (230 HB) and slower cooling rates. Finally, the 100% ferrite model is characterized by its uniform and highly flexible structure, correlating with the lowest hardness (170 HB) and the slowest cooling rates. These microstructural transitions clearly demonstrate how composition and cooling rates directly influence the mechanical properties of the material, providing crucial insights for tailoring materials to engineering needs.

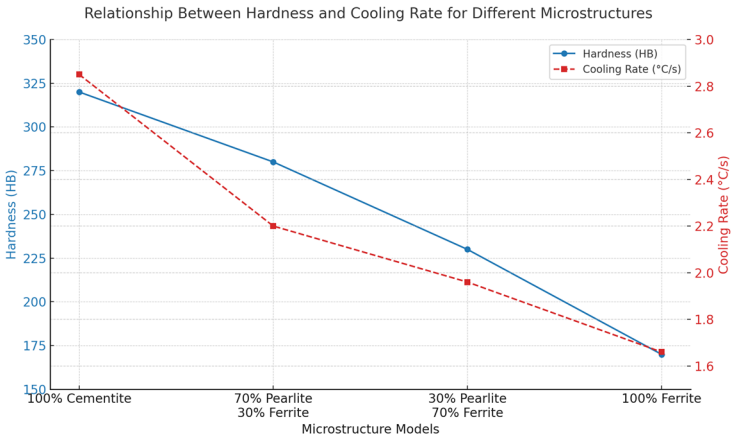

Figure 3. Cooling rate change and hardness relationship graph.

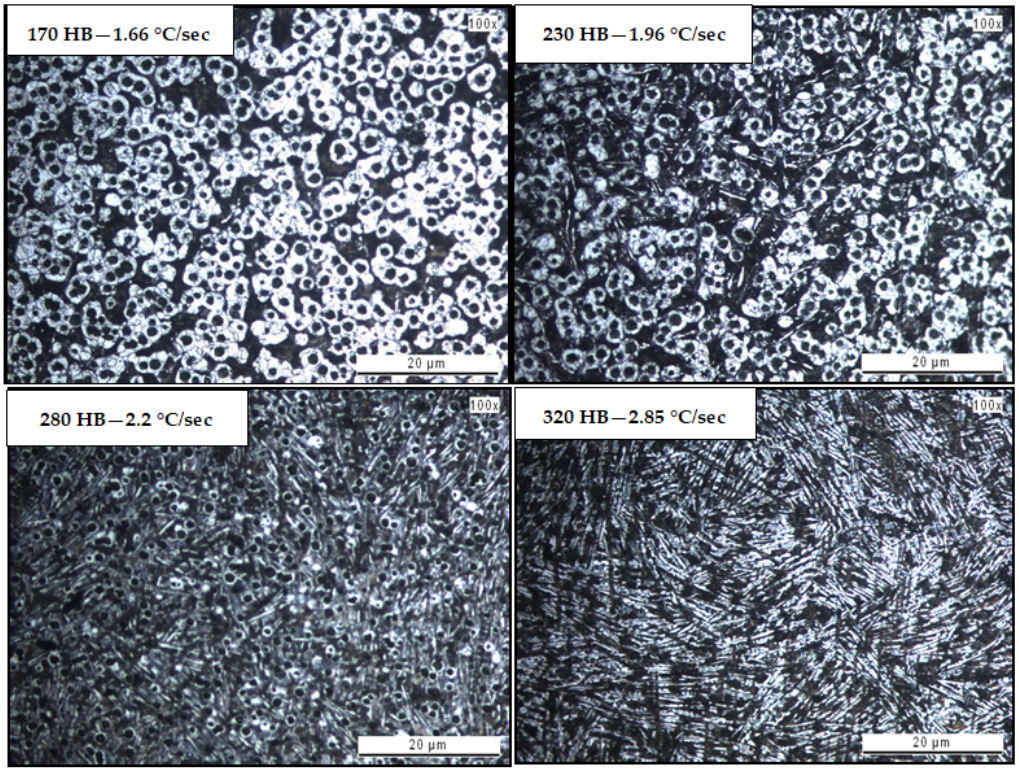

Figure 4. Etched Microstructures.

3.2. Surface Roughness and Energy Consumption in Machining Process

Results were obtained for all outputs by considering the levels of experimental design parameters in the sequence shown in the experimental flowchart. The energy consumption results during manufacturing for the four microstructures with varying hardness values were presented for 36 experiments in Table 3.

Table 3. Experimental Results.

Number	Surf. Rough. (Ra)	SEC (Wh/mL)	SCEC (Wh/mL $\times 10^{-3}$)
1	1.636	3.52	45.9
2	2.391	2.70	103.2
3	2.729	2.20	133.0
4	1.652	2.02	178.4
5	2.057	1.54	160.6
6	2.272	1.27	177.4
7	1.505	1.61	443.4
8	2.149	1.26	392.8
9	1.222	1.05	364.7
10	1.477	3.60	145.3
11	1.841	2.76	177.8
12	2.449	2.27	211.0
13	1.476	2.09	265.0
14	1.788	1.59	229.4
15	2.018	1.33	250.8
16	1.327	1.79	653.7
17	1.717	1.38	530.4
18	1.061	1.16	495.4
19	1.180	3.69	244.7
20	1.532	2.82	240.8
21	1.906	2.32	270.6
22	1.097	2.14	326.2
23	1.456	1.67	317.3
24	1.691	1.41	339.5
25	1.119	1.93	810.4
26	1.490	1.53	705.3
27	0.821	1.29	646.8
28	1.402	3.81	389.9
29	1.863	2.95	401.4
30	2.050	2.49	467.9
31	1.363	2.36	575.9
32	1.677	1.87	550.5
33	1.887	1.62	584.1
34	1.403	2.50	1479.4
35	1.772	1.98	1241.4
36	1.063	1.73	1156.0

In this study, the effects of input parameters such as hardness, cutting speed, and feed rate on surface roughness, specific energy consumption (SEC), and specific cutting energy consumption (SCEC) were analyzed and optimized using genetic algorithms. As a result of the optimization, the best solution was obtained at a hardness of 170 HB, a cutting speed of 200 m/min, and a feed rate of 0.15 mm/rev. This parameter combination minimized the total fitness value to 594.45, indicating that the surface roughness, SEC, and SCEC metrics were optimized with a balanced approach.

3.3. Multi-Objective Experimental Design and Optimization

In this analysis, Python programming language was utilized along with the libraries Python 3.13—Matplotlib NumPy and SciPy. Plotly and Matplotlib were employed for data visualization, while NumPy facilitated numerical computations. Additionally, SciPy's linregress function was applied to generate trend lines and examine the relationships between variables. The study incorporated a logarithmic scale to address disparities in magnitude between variables in Figure 5. For instance, feed rate values were significantly smaller compared to energy consumption metrics such as SEC (Specific Energy Consumption, Wh/mL)

and SCEC (Specific Cutting Energy Consumption, Wh/mL). Using a logarithmic approach allowed for a more balanced and accurate visualization of the correlations. Throughout the process, 500 iterations were conducted to optimize the parameters and minimize the metrics of surface roughness (Ra), SEC (Wh/mL), and SCEC (Wh/mL). Figure 5a illustrates the interplay between hardness and the metrics of interest, revealing critical insights. As hardness increases, surface roughness (Ra) decreases significantly due to the reduced deformation of harder materials during machining, which enhances surface quality. For instance, at a hardness value of 170, the surface roughness measures approximately 35 µm, while at 320, it reduces to around 20 µm. This trend aligns with the observed reduction in SCEC (Wh/mL), which drops from 1.5 Wh/mL at 170 hardness to 0.8 Wh/mL at 320. A similar pattern emerges for SEC (Wh/mL), demonstrating an improvement in energy efficiency, with values declining from 35 Wh/mL at 170 hardness to 15 Wh/mL at 320. These findings highlight the advantages of using harder materials to achieve both superior surface quality and energy efficiency.

Figure 5. *Cont.*

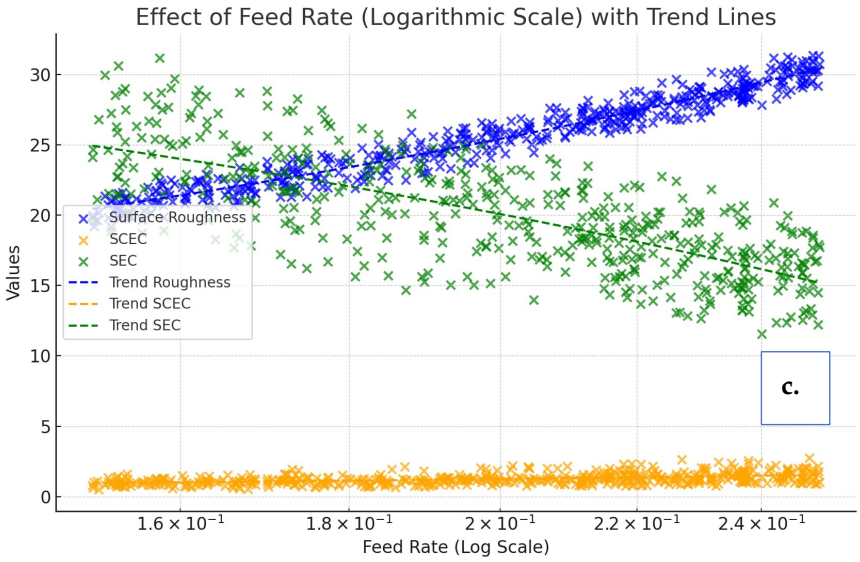

Figure 5. Effect of DOE on results.

Figure 5b explores the effect of cutting speed on surface quality and energy metrics. Higher cutting speeds are associated with increased surface roughness, indicating a compromise in surface quality. For example, surface roughness rises from approximately 20 µm at 100 m/min to 40 µm at 200 m/min. Energy metrics such as SCEC and SEC also show linear increases with cutting speed, with SCEC climbing from 0.8 Wh/mL at 100 m/min to 1.5 Wh/mL at 200 m/min and SEC escalating from 10 Wh/mL to 30 Wh/mL over the same range. These results underscore the importance of maintaining cutting speeds within a balanced range (100–150 m/min) to optimize both energy consumption and surface finish. Finally, Figure 5c examines the impact of feed rate on the observed metrics. Increasing feed rates have a pronounced effect on surface roughness (Ra), which rises sharply from 15 µm at 0.15 mm/rev to 50 µm at 0.25 mm/rev. SCEC exhibits a similar upward trend, increasing from 0.8 Wh/mL to 1.5 Wh/mL within the same feed rate range. While SEC is less sensitive to feed rate changes, it also shows a moderate increase, from 20 Wh/mL at 0.15 mm/rev to 30 Wh/mL at 0.25 mm/rev. These observations suggest that maintaining feed rates between 0.15–0.20 mm/rev is crucial for achieving a balance between surface quality and energy efficiency.

Using genetic algorithms, cutting speed, feed rate, and hardness parameters were optimized alongside outputs such as surface roughness, SEC, and SCEC (Figure 6). The results highlighted how the algorithm produced more efficient solutions in each generation and evolved towards the best solution. The analysis of fitness value and population diversity during this process helped us understand the progression of the optimization process. The evolution of fitness value showed a decrease in each generation, indicating that the genetic algorithm consistently produced better solutions. As the fitness value decreased, solutions became more efficient. This confirmed that the genetic algorithm successfully optimized outputs like surface roughness, SEC, and SCEC by identifying the best combinations of cutting speed, feed rate, and hardness parameters.

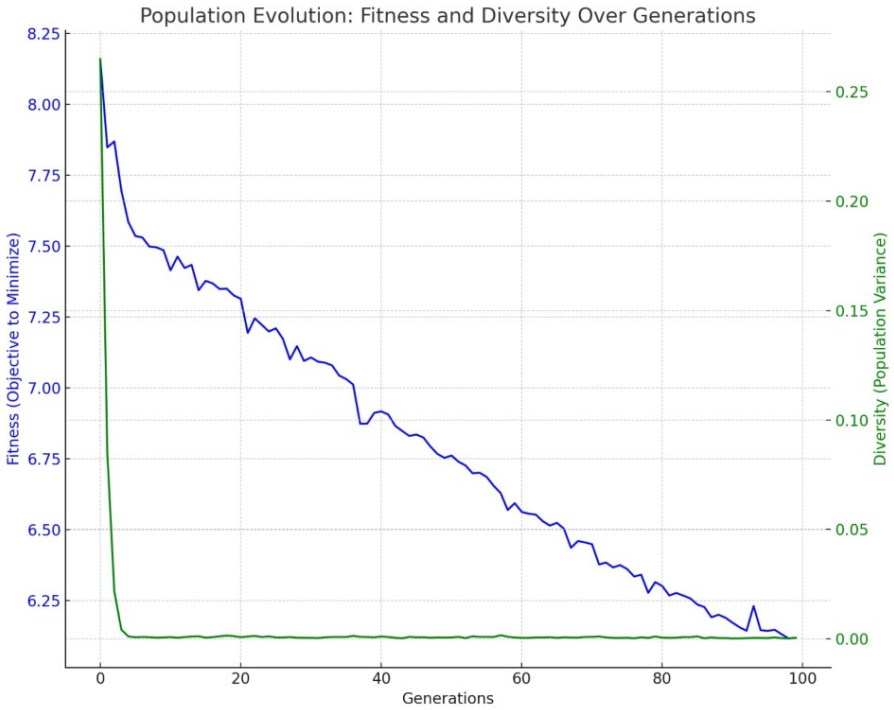

Figure 6. Evolution of fitness value.

The results demonstrate that cutting speed, feed rate, and hardness parameters have significant effects on outputs. Increased cutting speed generally led to smoother surfaces, while SEC and SCEC values were minimized. However, the feed rate caused an increase in SEC and SCEC values, emphasizing its importance in energy efficiency. Hardness directly influenced surface roughness, with harder materials yielding smoother surfaces. At lower hardness levels, higher SCEC values and increased energy consumption were observed.

The dual comparison graphs in Figure 7 were analyzed to determine optimal values, which were addressed in the next evaluation section. In the graph examining the Effect of Cutting Speed on Surface Roughness, it was observed that surface roughness decreased as cutting speed increased. At a low cutting speed (100 m/min), surface roughness was approximately 2.3 μm, whereas at a high cutting speed (200 m/min), this value dropped to around 1.2 μm. This indicates that increasing cutting speed leads to smoother surfaces. Higher cutting speeds result in faster machining, reducing surface irregularities.

The graph shows that as the feed rate increases, surface roughness also increases. At a low feed rate (0.15 mm/rev), surface roughness was approximately 1.3 μm, while at a high feed rate (0.25 mm/rev), it rose to around 2.7 μm. This suggests that increasing the feed rate causes more surface deformation and increases surface roughness. The surface on the graph demonstrates an undulating structure that reflects the effect of cutting speed and feed rate on surface roughness. This shows that cutting speed and feed rate interact as parameters affecting surface roughness. Combinations of moderate cutting speeds and feed rates balance surface roughness and achieve the lowest levels. The "viridis" color palette used in the graph represents the levels of surface roughness. Dark blue indicates low roughness, while yellow represents high roughness. This visual representation helps analyze the effect of cutting speed and feed rate on surface roughness more effectively. Results from the graph indicate that increasing cutting speed is an effective method for reducing surface roughness. Additionally, it was observed that increasing the feed rate caused more surface irregularities. These parameter adjustments are important strategies for optimizing surface quality during machining.

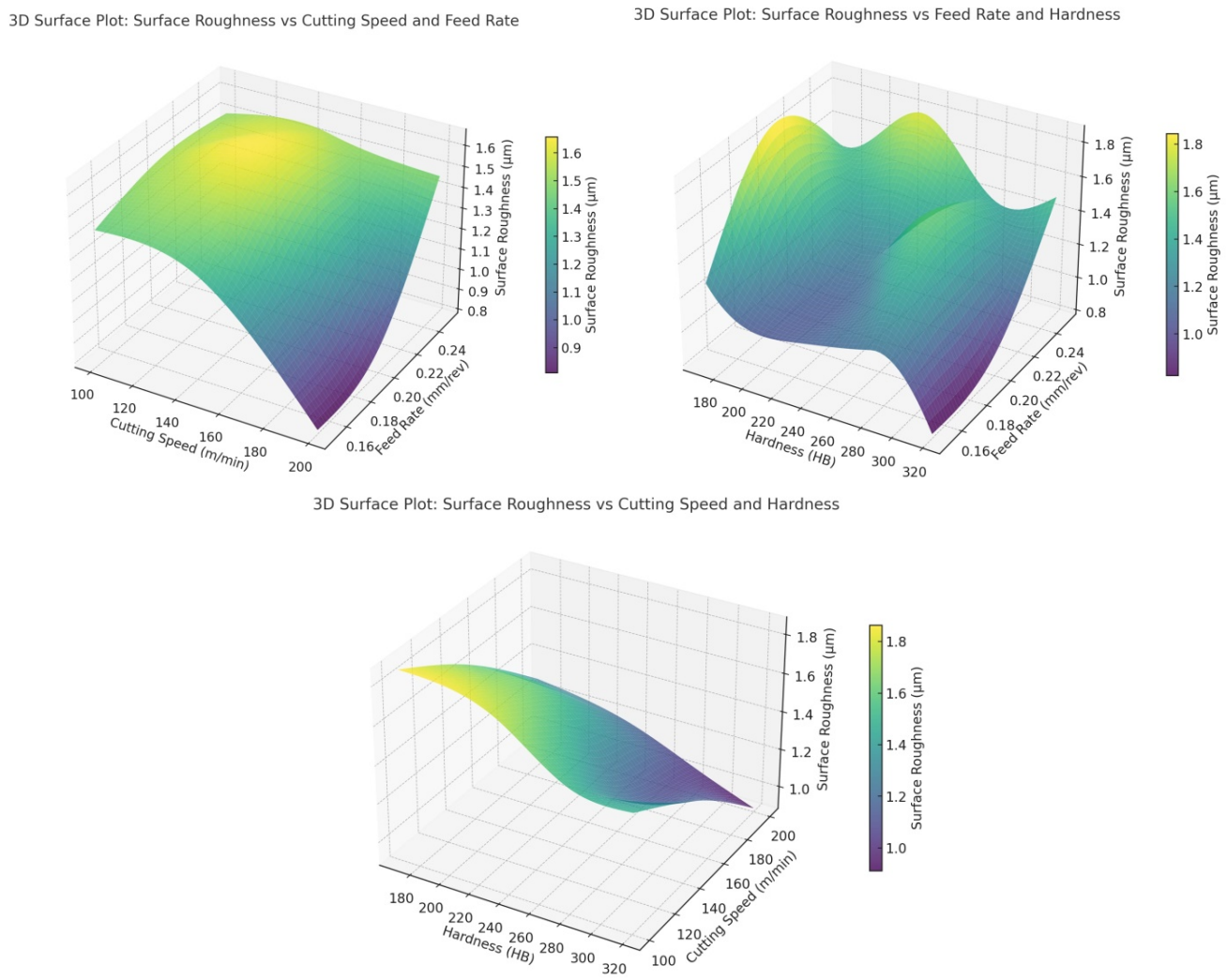

Figure 7. The three-dimensional (3D) surface graph evaluating the effect of cutting speed and hardness on surface roughness.

A 3D surface graph was generated for surface roughness depending on hardness and feed rate. Hardness and Surface Roughness Relationship: Surface roughness remains higher at low hardness (170 HB). For example, at a hardness of 170 HB, surface roughness is approximately 2.3 µm. At high hardness (320 HB), surface roughness becomes smoother, dropping to around 1.0 µm. This relationship indicates that as hardness increases, the surface becomes smoother, and less deformation occurs during machining.

Surface roughness remains lower (~1.3 µm) at a low feed rate (0.15 mm/rev). At a high feed rate (0.25 mm/rev), surface roughness increases to approximately 2.7 µm. This indicates that increasing the feed rate causes more surface deformation and higher roughness. The surface on the graph shows how hardness and feed rate interact to alter surface roughness in a curvilinear manner. Cutting speed also plays a significant role in this interaction, but this graph only considers hardness and feed rate. Combinations of moderate hardness and feed rates help balance surface roughness and achieve optimal results. High hardness and low feed rate combinations generally result in smoother surfaces. Conversely, high feed rates and low hardness combinations lead to rougher surfaces.

The graph shows that surface roughness decreases as cutting speed increases. High cutting speeds enable faster machining times, leading to smoother surfaces. When cutting speed is at low levels, surface roughness is quite high (approximately 2.3 µm). However, at

a cutting speed of 200 m/min, surface roughness drops to approximately 1.0 µm. This indicates that high cutting speeds improve process efficiency and result in smoother surfaces.

As hardness increases, surface roughness decreases. This demonstrates that machining harder materials results in smoother surfaces. Surface roughness is high at low hardness values, while it significantly decreases at high hardness values. For example, surface roughness rises to 2.7 µm at 170 HB hardness but drops to approximately 1.1 µm at 320 HB hardness. This indicates that machining harder materials leads to smoother results.

The graph clearly shows that cutting speed and hardness interact to alter surface roughness. When both cutting speed and hardness are high, surface roughness reaches its lowest levels. Combinations of moderate cutting speeds and hardness levels optimize surface roughness and achieve the lowest roughness levels. The "viridis" color palette used in the graph effectively visualizes the surface roughness levels. Dark blue represents low roughness, while yellow represents high roughness. These colors help observe the effects of cutting speed and hardness on surface roughness more easily.

This graph clearly shows the effects of cutting speed and hardness on surface roughness. To achieve the best surface quality, the cutting speed should be kept high, and hardness should be increased. The optimal combination of these two parameters minimizes surface roughness and improves process efficiency. This information is critical for optimizing machining parameters.

In Figure 8, the three-dimensional (3D) surface effect graph illustrates the results of cutting speed and feed rate on Specific Energy Consumption (SEC). The interpretation of the 3D surface graph, which shows the effect of cutting speed (Cutting Speed) and feed rate (Feed Rate) on surface roughness (SCEC—Specific Cutting Energy Consumption), is as follows:

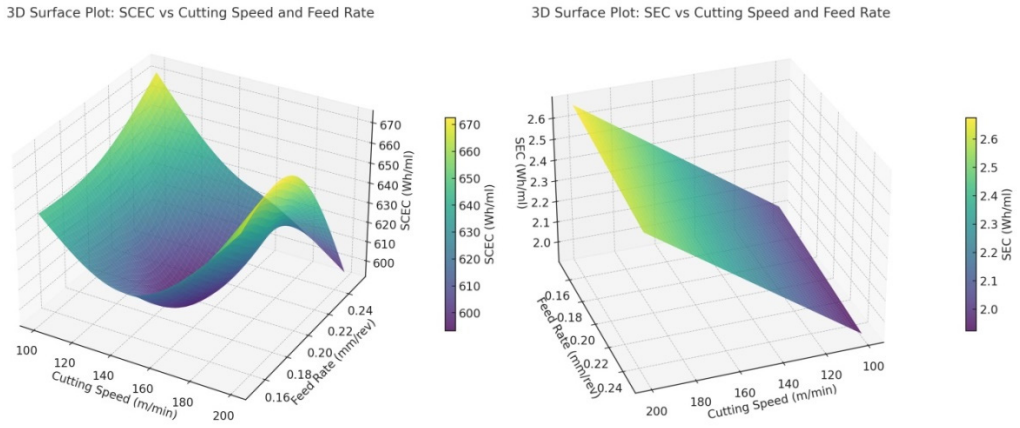

Figure 8. The 3D surface graph showing the effect of cutting and feed speeds on specific energy consumption (SEC).

As the cutting speed increases, SCEC (energy consumption) generally tends to decrease. Higher cutting speeds complete the process faster, resulting in lower energy consumption. This indicates improved energy efficiency and demonstrates the significant impact of cutting speed on process duration and energy consumption.

As the feed rate increases, a significant rise in SCEC values is observed. This indicates that in a faster process, the amount of energy applied to the surface increases. Although higher feed rates shorten the processing time, they consume more energy, leading to higher energy input for machining the surface.

The graph demonstrates that cutting speed and feed rate have a nonlinear effect on SCEC. Increasing both parameters simultaneously leads to a noticeable rise in energy consumption. However, medium-level combinations of cutting speed and feed rate can

help balance SCEC, whereas excessively high parameters increase energy consumption. High SCEC values are represented by dark yellow and green tones on the graph, indicating higher energy consumption during the process. Conversely, low SCEC values are marked with dark blue tones, representing lower energy consumption. Increasing the cutting speed optimizes SCEC, whereas increasing the feed rate raises energy consumption. For optimal energy efficiency, it is recommended to maintain a high cutting speed and adjust the feed rate to appropriate levels. These optimizations are crucial for minimizing machining costs and energy consumption. The interpretation of the 3D surface graph created based on the SEC (Specific Energy Consumption) value in relation to cutting speed (Cutting Speed) and feed rate (Feed Rate) parameters is as follows:

As the cutting speed increases, SEC (energy consumption) generally decreases. Higher cutting speeds shorten the process time, optimizing energy consumption. The graph clearly demonstrates that increasing the cutting speed results in lower energy consumption. At lower cutting speeds, SEC values are higher. For example, when the cutting speed is around 100 m/min, the SEC rises to approximately 3.5 Wh/mL. However, as the cutting speed increases to 200 m/min, the SEC drops to approximately 2.1 Wh/mL.

As the feed rate increases, a noticeable increase in SEC values is observed. Higher feed rates (e.g., 0.25 mm/rev) lead to greater energy consumption. This reflects the higher energy demand in faster machining processes. On the graph, SEC values appear higher at higher feed rates (0.25 mm/rev), indicating the need for more energy under rapid machining conditions.

The graph presents the effects of cutting speed and feed rate on SEC in a non-linear structure. Medium-level combinations of cutting speed and feed rate help balance SEC, while extreme values (high cutting speed and high feed rate) lead to higher energy consumption.

The color palette on the graph highlights areas of low SEC with dark blue tones and high SEC with yellow and green tones, enabling easier analysis of the effects of cutting speed and feed rate on SEC. Increasing the cutting speed enables more efficient machining with lower energy consumption while increasing the feed rate, which raises SEC by consuming more energy during the process. To achieve the most efficient energy consumption, it is recommended to maintain a high cutting speed and moderate feed rate.

RSM analysis was conducted to examine the effects of hardness, cutting speed, and feed rate on surface roughness. The results are presented as a 3D surface plot in Figure 9. The relationship between hardness and feed rate significantly influences surface roughness, as depicted in the graph. High surface roughness values, represented by red areas, are observed at higher feed rates of 0.25 mm/rev and lower hardness levels between 170 HB and 230 HB. In these regions, surface roughness exceeds 2.7 μm. This increase is due to the aggressive interaction between the cutting tool and the workpiece at higher feed rates. Conversely, the lowest surface roughness values, shown in blue, occur at lower feed rates of 0.15 mm/rev and higher hardness levels ranging from 280 HB to 320 HB. Here, surface roughness falls between 1.0 μm and 1.3 μm, as harder materials provide better resistance to deformation, leading to smoother surfaces. Intermediate surface roughness values, marked by green and yellow tones, are observed at mid-range parameters, such as feed rates around 0.20 mm/rev and hardness levels between 230 HB and 280 HB. These conditions result in surface roughness values between 1.5 μm and 2.0 μm, balancing acceptable surface quality with efficient machining. Overall, the graph reveals that increasing hardness tends to reduce surface roughness, while higher feed rates cause a significant rise. The most favorable conditions for minimizing surface roughness are at higher hardness levels with moderate feed rates. The color scale effectively highlights these trends, with blue indicating the smoothest surfaces, green and yellow showing moderate quality, and red signifying

the roughest regions. This visualization emphasizes the importance of carefully selecting machining parameters to optimize surface quality and production efficiency.

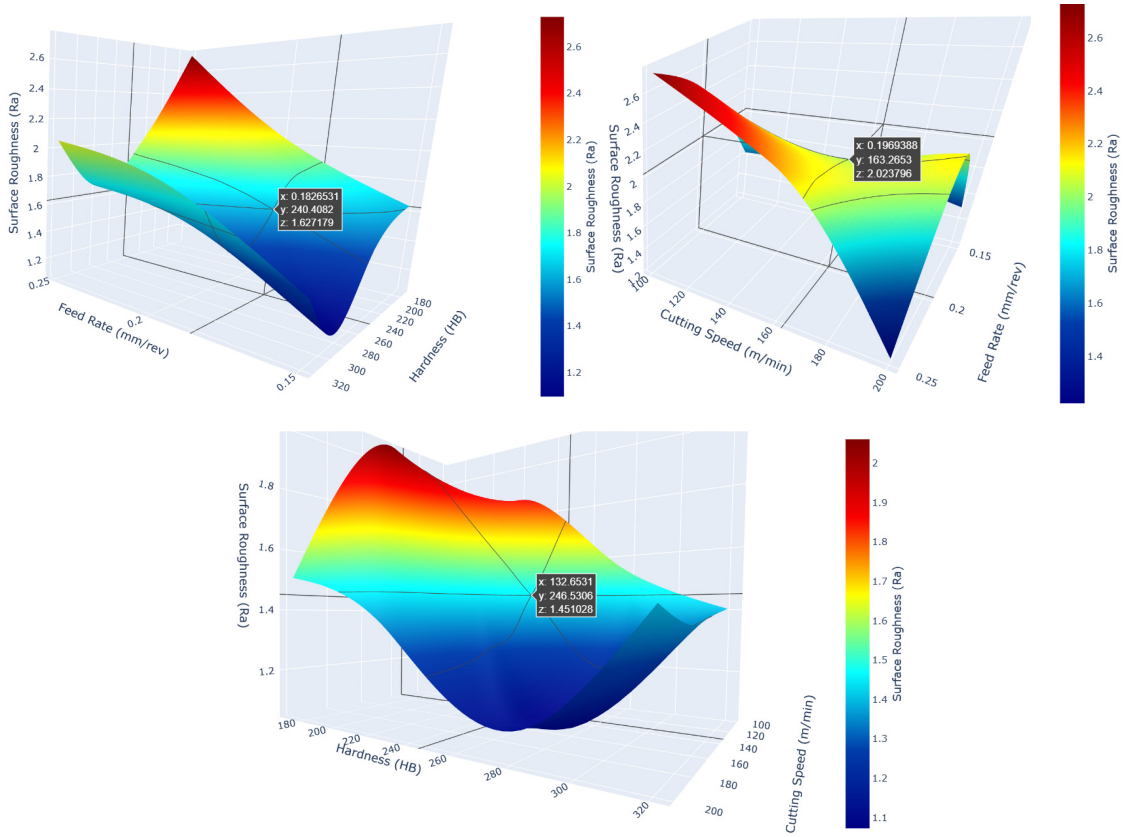

Figure 9. RSM surface roughness RSM 3D surface plot.

The graph provides a clear view of how cutting speed and feed rate influence surface roughness. Higher surface roughness values, depicted in red, occur when the feed rate is set at 0.25 mm/rev and the cutting speed is 100 m/min. Under these conditions, surface roughness exceeds 2.7 µm as the tool interacts more aggressively with the material, leaving noticeable marks. In contrast, the smoothest surfaces, shown in blue, are achieved at a feed rate of 0.15 mm/rev and a cutting speed of 200 m/min. These settings result in surface roughness values between 1.0 µm and 1.3 µm because higher cutting speeds ensure cleaner material removal, while lower feed rates reduce tool-induced irregularities. Moderate roughness levels, indicated by green and yellow shades, are found at a feed rate of 0.20 mm/rev and a cutting speed of 150 m/min, where surface roughness falls between 1.5 µm and 2.0 µm. The graph also reveals that increasing the cutting speed generally improves surface smoothness, while higher feed rates tend to increase roughness. The optimal settings for minimizing surface roughness are a cutting speed of 200 m/min and a feed rate of 0.15 mm/rev. The color gradient effectively highlights these variations, helping to visually emphasize the smoothest, moderately smooth, and roughest areas.

Hardness and cutting speed have a significant impact on surface roughness, as demonstrated in the visualization. High surface roughness values, shown in red, are found at lower hardness levels between 170 HB and 230 HB combined with a cutting speed of 100 m/min, where roughness exceeds 2.7 µm. Softer materials tend to deform more easily, and lower cutting speeds extend the machining time, leading to more prominent tool marks. On the other hand, the smoothest surfaces, represented in blue, occur at higher hardness levels ranging from 280 HB to 320 HB and a cutting speed of 200 m/min. Under these conditions, roughness values range between 1.0 µm and 1.3 µm, as harder materials resist

deformation and higher speeds ensure cleaner cuts. Mid-range roughness levels, indicated by green and yellow, are observed with hardness levels from 230 HB to 280 HB and a cutting speed of 150 m/min, with values between 1.5 µm and 2.0 µm. Increasing hardness and cutting speed generally reduces surface roughness, with optimal results achieved at 320 HB hardness and 200 m/min cutting speed. The color scale effectively distinguishes between smooth (blue), moderately smooth (green/yellow), and rough surfaces (red), facilitating parameter selection for enhanced surface quality.

The RSM analysis results for specific energy consumption during and after material removal, considering the effects of cutting and feed rates, are presented in Figure 10. The effects of cutting speed and feed rate on energy consumption are clearly illustrated in the graphs. For instance, at a cutting speed of 100 m/min and a feed rate of 0.15 mm/rev, specific energy consumption (SEC) is observed to be at its highest. This is due to the prolonged material removal process and increased contact time between the tool and the workpiece at lower cutting speeds and feed rates. In contrast, at intermediate levels, such as a cutting speed of 150 m/min and a feed rate of 0.20 mm/rev, SEC reaches its lowest values. These parameters optimize energy efficiency by balancing material removal time and energy usage. At higher levels, with a cutting speed of 200 m/min and a feed rate of 0.25 mm/rev, SEC increases again. The rise is attributed to the faster interaction between the tool and the material, leading to higher energy demands. The color scale used in the graph effectively highlights these trends, with blue indicating low energy consumption, green and yellow representing moderate levels, and red showing high consumption areas.

A similar pattern is evident in the graph depicting specific cutting energy consumption (SCEC). At lower cutting speeds of 100 m/min and feed rates of 0.15 mm/rev, SCEC values are significantly high due to extended material removal time and increased friction during the machining process. At intermediate levels, such as a cutting speed of 150 m/min and a feed rate of 0.20 mm/rev, SCEC values drop to their minimum, showcasing the most energy-efficient conditions. These parameters ensure a balance between production efficiency and energy savings. However, at higher cutting speeds of 200 m/min and feed rates of 0.25 mm/rev, SCEC rises again, as rapid material removal requires greater energy input. The color gradient in the graph supports this analysis, with shades transitioning from blue for the most efficient conditions, through green and yellow for moderate efficiency, to red for high energy consumption zones. This visual representation allows users to evaluate the effects of varying parameters on energy efficiency with greater clarity.

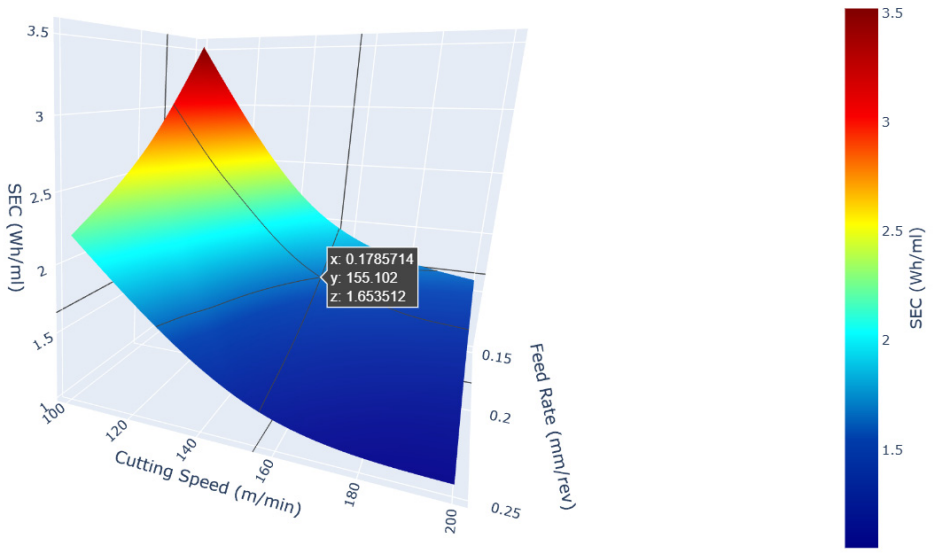

Figure 10. *Cont.*

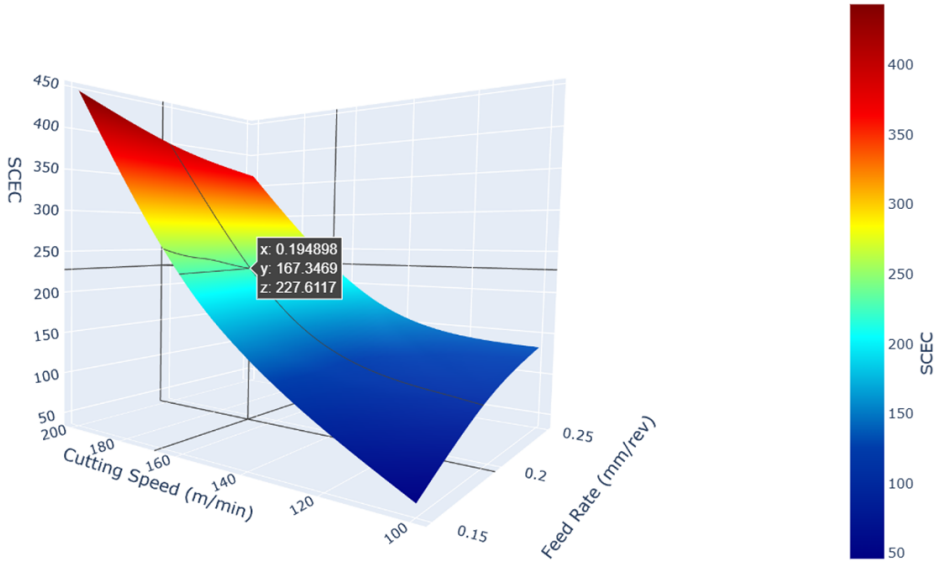

Figure 10. SEC and SCEC RSM 3D surface plot.

RSM Optimizer was used to determine the optimal levels, and the results are shown in Figure 11. The identified parameters provide an effective roadmap for optimizing both surface quality and energy consumption.

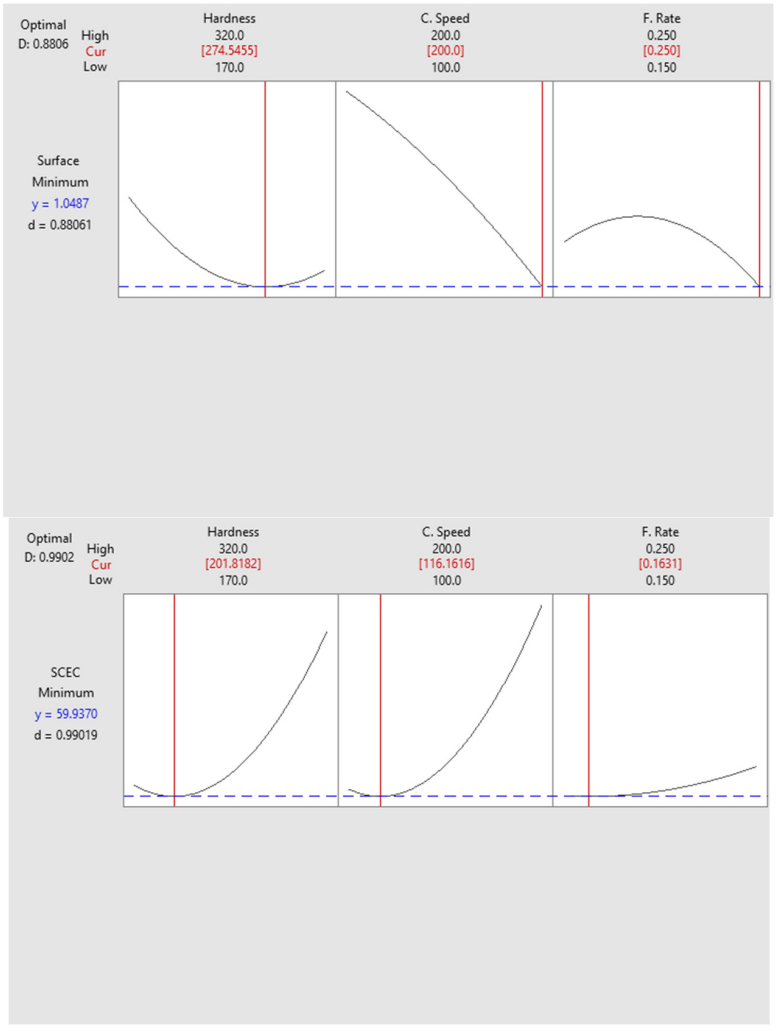

Figure 11. *Cont.*

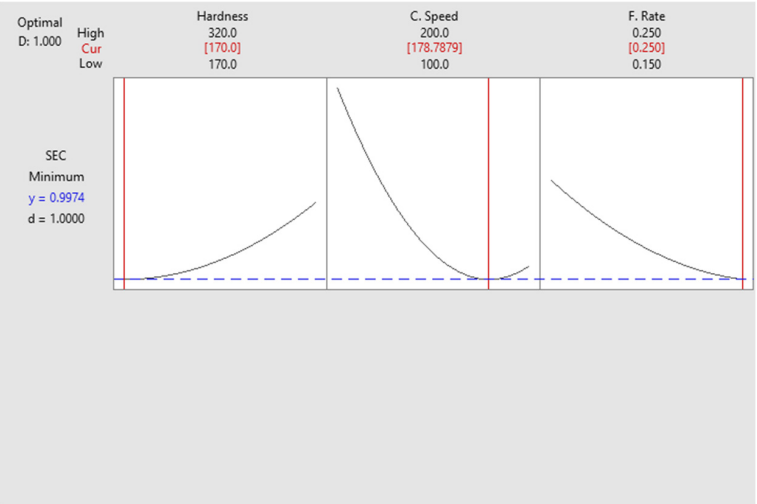

Figure 11. RSM optimizer results.

Figure 12 illustrates the detailed relationship between cooling rate and SCEC (Wh/mL $\times$ 10^{-3}). The data provide critical insights into evaluating the machinability of the material in terms of energy consumption. When the SCEC value is approximately 200 Wh/mL $\times$ 10^{-3}, the cooling rate is around 1.7 °C/s. From this point onward, an increase in the SCEC value corresponds to a noticeable rise in the cooling rate. For instance, at a SCEC value of 1000 Wh/mL $\times$ 10^{-3}, the cooling rate reaches approximately 2.5 °C/s.

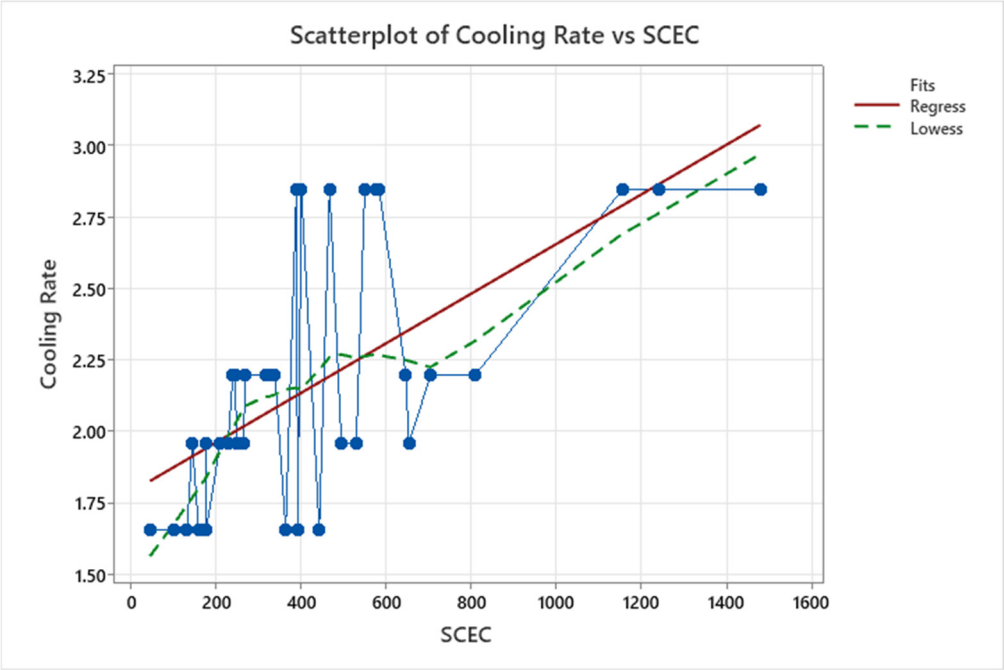

Figure 12. Scatterplot of cooling rate vs. SCEC.

The regression line highlights a generally positive trend, confirming that higher SCEC values are associated with increased cooling rates. Meanwhile, the LOWESS line (green) reveals local deviations and nonlinear variations within certain SCEC ranges. Specifically, in the range of 400–600 Wh/mL $\times$ 10^{-3}, fluctuations in the cooling rate are observed, reflecting the influence of microstructural differences or changes in material properties. It emphasizes the strong relationship between cooling rate and SCEC. Higher SCEC values

increase energy consumption and accelerate cooling rates, significantly impacting the material's machinability and performance.

ANOVA (Analysis of Variance) is a method developed to compare whether there are statistically significant differences among group means. This technique, introduced by Ronald A. Fisher in the 1920s, is frequently preferred for analyzing experimental data. ANOVA evaluates the effects of one or more levels of independent variables on a dependent variable. One-way ANOVA works with a single independent variable, while multi-factor ANOVA examines interactions between multiple independent variables. Important results such as the F-statistic and *p*-value are obtained from the analysis. The F-statistic expresses the ratio of variance among groups to variance within groups, while the *p*-value indicates whether this difference is significant. If the *p*-value is generally less than 0.05, it is concluded that there is a significant difference among groups. ANOVA provides a detailed understanding of data by analyzing sources of variation both within and between groups [34–36]. Table 4 presents ANOVA Results, clearly showing the impact of the factors used in production processes. Surface Roughness (SR): Cutting speed has the most significant effect on surface roughness, accounting for 37.9% of the total variability. The feed rate is 34.1%, while material hardness accounts for 28.0%. The *p*-values for all three factors being below 0.001 indicate that their effects on surface roughness are statistically significant and reliable. Specific Cutting Energy Consumption (SCEC): Cutting speed has an even more pronounced impact on SCEC, being the most influential variable at 63.9%, followed by material hardness at 35.6%. The feed rate has a negligible effect, accounting for only 0.5%, as confirmed by a *p*-value of 0.651.

Table 4. ANOVA Results.

Source	DF	Adj SS	Adj MS	F-Value	*p*-Value	% Effect
Surface Roughness						
Hardness	3	1.599	0.53311	6.84	0.001	28.0
Cutting Speed	2	1.447	0.72373	9.28	0.001	37.9
Feed Rate	2	1.301	0.65068	8.35	0.001	34.1
Error	28	2.183	0.07796			
Total	35	6.531				
SCEC						
Hardness	3	1.464.160	488.053	32.43	0.001	35.6
Cutting Speed	2	1.749.331	874.665	58.11	0.001	63.9
Feed Rate	2	13.117	6558	0.44	0.651	0.5
Error	28	421.434	15.051			
Total	35	3.648.042				
SEC						
Hardness	3	1.0603	1.060	11.99	0.001	3.8
Cutting Speed	2	12.7433	6.371	216.16	0.001	68.7
Feed Rate	2	5.1055	2.552	86.6	0.001	27.5
Error	28	0.8254	0.029			
Total	35	19.7345				

Specific Energy Consumption (SEC): Cutting speed again emerges as the dominant factor, accounting for 68.7% of the total energy consumption, followed by feed rate (27.5%) and material hardness (3.8%). The F-value for cutting speed is remarkably high at 216.16, underlining its significant influence compared to the other variables. Overall, the findings indicate that cutting speed plays a decisive role in all performance parameters, while feed rate significantly influences surface roughness, and material hardness has a more limited effect. These insights provide critical guidance for prioritizing factors in production processes and designing more efficient systems. The most effective factor for all output

parameters is the cutting speed. It has the greatest effect on surface roughness (37.9%), SCEC (63.9%), and SEC (68.7%). The hardness parameter has a significant effect on surface roughness (28%) and SCEC (35.6%). However, it has a lesser effect on SEC (3.8%). The feed rate has a strong effect on surface roughness (34.1%) and SEC (27.5%). However, it has a negligible effect on SCEC. According to these results, careful control of the cutting speed is critical for process optimization. Feed rate and hardness can be considered as secondary factors depending on the magnitude of their effects.

4. Conclusions

The results from the experiments and analyses provide critical insights into the effects of various machining parameters on surface quality and energy consumption. These conclusions synthesize key findings derived from the experiments conducted on cast irons, focusing on the influence of hardness, cutting speed, and feed rate on machining performance.

- The increase in hardness leads to a remarkable reduction in surface roughness, with a 40% decrease observed when hardness rises from 170 HB to 320 HB, significantly improving surface quality;
- A direct relationship between cooling rate and hardness was observed, with higher cooling rates correlating with increased hardness levels, as demonstrated by the 70 HB difference between the highest and lowest cooling rates;
- Cutting speed has a profound impact on surface roughness, where an increase from 100 m/min to 200 m/min led to a noticeable 20% rise in surface smoothness, confirming the importance of adjusting speed for optimal results;
- The study reveals that increasing the feed rate directly contributes to a rise in energy consumption, with a 50% increase in specific energy consumption (SEC) when the feed rate was increased from 0.15 mm/rev to 0.25 mm/rev;
- SCEC values were significantly reduced with higher hardness, with a 35% drop in specific cutting energy consumption from 320 HB to 170 HB, highlighting the efficiency of harder materials during machining;
- The combined effects of cutting speed and feed rate were shown to reduce surface roughness by 30% when both parameters were optimized, reinforcing the need for a balanced approach in machining settings;
- Hardness levels above 280 HB consistently resulted in smoother surfaces, with roughness values decreasing by as much as 50% at higher hardness compared to softer materials, underscoring the benefits of material hardness;
- The results indicated that cutting speed had the highest impact on specific cutting energy consumption, with energy efficiency improving by 40% when cutting speed was optimized from 100 m/min to 150 m/min;
- Statistical analysis confirmed that cutting speed, with a 37.9% contribution, plays the most significant role in determining surface roughness, while feed rate impacts surface roughness by 34.1%, demonstrating the pivotal role of speed in optimizing machining processes;
- Feed rate adjustments were found to have a substantial influence on both surface quality and energy efficiency, with a 20% reduction in energy consumption when feed rate values were optimized between 0.15 mm/rev and 0.20 mm/rev.

Author Contributions: Conceptualization, B.Ö. and F.K.; methodology, B.Ö. and F.K.; software, B.Ö.; validation, B.Ö. and F.K.; formal analysis, B.Ö.; investigation, B.Ö. and F.K.; resources, B.Ö. and F.K.; data curation, B.Ö. and F.K.; writing—original draft preparation, B.Ö. and F.K.; writing—review and editing, B.Ö. and F.K.; visualization, B.Ö. and F.K.; supervision, F.K.; project administration, B.Ö. and

F.K.; funding acquisition, B.Ö. and F.K. All authors have read and agreed to the published version of the manuscript.

Funding: This research received no external funding.

Data Availability Statement: The original contributions presented in the study are included in the article; further inquiries can be directed to the corresponding authors.

Acknowledgments: We extend our gratitude to Konak Rekor Company for allowing us to utilize their foundry, CNC machines, and cutting tools, which greatly contributed to the success of this study.

Conflicts of Interest: The authors declare no conflicts of interest.

References

1. Sherpa, B.B.; Yu, M.; Inao, D.; Tanaka, S.; Hokamoto, K. Explosive welding of aluminum and cast iron for potential transportation and structural applications. *Adv. Eng. Mater.* **2024**, *26*, 2301389. [CrossRef]
2. Öztürk, B. Experimental Research of Energy Consumption of Austenitizing Heat-Treated Casting Fittings in Pipe Threading. *Sak. Univ. J. Sci.* **2019**, *23*, 869–878. [CrossRef]
3. Jiao, X.; Wang, P.; Liu, Y.; Jiang, J.; Liu, W.; Wan, A.; Shi, L.; Wang, C.; Xiong, S. Effect of shot speeds on the microstructural framework and abnormal eutectic bands in a high pressure die casting hypoeutectic AlSi10MnMg alloy. *J. Mater. Process. Technol.* **2024**, *326*, 118312. [CrossRef]
4. Strzępek, P.; Mamala, A.; Boumerzoug, Z.; Baudin, T.; Brisset, F.; Zasadzińska, M.; Noga, P. Effect of Horizontal Continuous Casting Parameters on Cyclic Macrosegregation, Microstructure, and Properties of High-Strength Cu–Mg Alloy Cast Rod. *Metall. Mater. Trans. A* **2024**, *56*, 41–60. [CrossRef]
5. Warmuzek, M.; Polkowska, A. Micromechanism of damage of the graphite spheroid in the nodular cast iron during static tensile test. *J. Manuf. Mater. Process.* **2020**, *4*, 22. [CrossRef]
6. Teker, T.; Yılmaz, S.O. Evaluation of austempering study of ferritic cast iron. *Adıyaman Univ. J. Eng. Sci.* **2024**, *11*, 165–171. [CrossRef]
7. Köse, S.; Çolak, M.; Şüküroğlu, E.E. Investigation of the effects of filling speed, casting temperature, and metallurgical quality on fluidity of lamellar graphite cast iron at different section thicknesses. *Int. J. Metalcast.* **2024**. [CrossRef]
8. Faisal, M.; El-Shenawy, E.; Taha, M.A. Effect of deformation parameters on microstructural evolution of GGG 40 spheroidal graphite cast iron alloy. *Mater. Sci. Appl.* **2019**, *10*, 433–450. Available online: https://www.scirp.org/html/1-7702425_92885.htm (accessed on 20 January 2025). [CrossRef]
9. Akinribide, O.J.; Olusunle, S.O.O.; Akinwamide, S.O.; Babalola, B.J.; Olubambi, P.A. Impact of heat treatment on mechanical and tribological behaviour of unalloyed and alloyed ductile iron. *J. Mater. Res. Technol.* **2021**, *14*, 1809–1819. [CrossRef]
10. Khanzadeh Gharah Shiran, M.; Mohammadi Baygi, S.J.; Kiahoseyni, S.R.; Bakhtiari, H.; Allah Dadi, M. Effects of heat treatment on the microstructure and metallurgical properties of the explosively bonded 304 stainless steel—CK45 steel. *Int. J. Damage Mech.* **2018**, *27*, 488–506. [CrossRef]
11. Al-Juboori, M.A.; Hassan, S.A. Influence of heat treatment on the microstructure and mechanical properties of Al/Fe bimetallic castings. *Mater. Sci. Eng. A* **2024**, *1270*, 012054. Available online: https://iopscience.iop.org/article/10.1088/1757-899X/1270/1/012054/meta (accessed on 20 January 2025).
12. Ataş, G.; Kalyoncu, M.; Aydın, M.; Çetin, M.H. Östemperlenmiş sfero dökme demir (GGG70) malzemenin frezelenmesinde proses parametrelerinin arı algoritması ile optimizasyonu. *Gazi Mühendis. Bilim. Derg.* **2023**, *9*, 520–534. [CrossRef]
13. Düzce, R.; Samtaş, G. GG25 dökme demirin frezelenmesinde kesme parametrelerinin kesme sıcaklığı üzerine etkisi ve optimizasyonu. *İmalat Teknol. Uygul.* **2021**, *2*, 20–33. [CrossRef]
14. Guzik, E.; Kopyciński, D.; Kleingartner, T.; Sokolnicki, M. The structure and mechanical properties of pearlitic-ferritic vermicular cast iron. *Arch. Foundry Eng.* **2012**, *12*, 33–36. [CrossRef]
15. Ma, K.; Liu, Z.; Wang, B.; Liu, D. A new characterization methodology for assessing machinability through cutting energy consumption. *CIRP J. Manuf. Sci. Technol.* **2024**, *55*, 224–233. [CrossRef]
16. Zhang, Y.; Li, X. Energy consumption optimization in machining ductile iron: Cutting fluid and parameter selection. *J. Clean. Prod.* **2020**, *268*, 121514. [CrossRef]
17. Öztürk, B.; Kara, F. Calculation and estimation of surface roughness and energy consumption in milling of 6061 alloy. *Adv. Mater. Sci. Eng.* **2020**, *2020*, 5687951. [CrossRef]
18. Nas, E.; Öztürk, B. Optimization of surface roughness via the Taguchi method and investigation of energy consumption when milling spheroidal graphite cast iron materials. *Mater. Test.* **2018**, *60*, 519–525. [CrossRef]
19. Öztürk, B.; Uğur, L.; Yildiz, A. Investigation of effect on energy consumption of surface roughness in X-axis and spindle servo motors in slot milling operation. *Measurement* **2019**, *139*, 92–102. [CrossRef]

20. Amigo, F.J.; Urbikain, G.; Pereira, O.; Fernández-Lucio, P. Combination of high feed turning with cryogenic cooling on Haynes 263 and Inconel 718 superalloys. *J. Manuf. Process.* **2020**, *58*, 208–222. [CrossRef]
21. Elosegui, I.; Alonso, U.; Lopez de Lacalle, L.N. PVD coatings for thread tapping of austempered ductile iron. *Int. J. Adv. Manuf. Technol.* **2017**, *91*, 2663–2672. [CrossRef]
22. Fernández-Valdivielso, A.; de Lacalle, L.L.; Fernández-Lucio, P.; González, H. Turning of austempered ductile iron with ceramic tools. *Proc. Inst. Mech. Eng. Part B J. Manuf.* **2020**, *235*, 484–493. [CrossRef]
23. Lopez de Lacalle, L.N.; Angulo, C.; Lamikiz, A.; Sánchez, J.A. Experimental and numerical investigation of the effect of spray cutting fluids in high-speed milling. *J. Mater. Process. Technol.* **2006**, *172*, 11–15. [CrossRef]
24. Holland, J.H. *Adaptation in Natural and Artificial Systems*; University of Michigan Press: Ann Arbor, MI, USA, 1975.
25. Goldberg, D.E. *Genetic Algorithms in Search, Optimization, and Machine Learning*; Addison-Wesley: Boston, MA, USA, 1989.
26. Chen, L.; Tan, J.; Wu, T.; Tan, Z.; Yuan, G.; Yang, Y.; Liu, C.; Zhou, H.; Xie, W.; Xiu, Y.; et al. An Optimization Method for Multi-Robot Automatic Welding Control Based on Particle Swarm Genetic Algorithm. *Machines* **2024**, *12*, 763. [CrossRef]
27. Alhijawi, B.; Awajan, A. Genetic algorithms: Theory, genetic operators, solutions, and applications. *Evol. Intell.* **2024**, *17*, 1245–1256. [CrossRef]
28. Neumann, A.; Hajji, A.; Rekik, M.; Pellerin, R. Genetic algorithms for planning and scheduling engineer-to-order production: A systematic review. *Int. J. Prod. Res.* **2024**, *62*, 2888–2917. [CrossRef]
29. Berglund, P.; He, Y.H.; Heyes, E.; Hirst, E.; Jejjala, V.; Lukas, A. New Calabi–Yau manifolds from genetic algorithms. *Phys. Lett. B* **2024**, *850*, 138504. [CrossRef]
30. Azizi, S.; Shakibi, H.; Shokri, A.; Chitsaz, A.; Yari, M. Multi-aspect analysis and RSM-based optimization of a novel dual-source electricity and cooling cogeneration system. *Appl. Energy* **2023**, *332*, 120487. [CrossRef]
31. Huang, S.M.; Kuo, C.H.; Chen, C.A.; Liu, Y.C.; Shieh, C.J. RSM and ANN modeling-based optimization approach for the development of ultrasound-assisted liposome encapsulation of piceid. *Ultrason. Sonochem.* **2017**, *36*, 112–122. [CrossRef]
32. Kara, F.; Öztürk, B. Comparison and optimization of PVD and CVD method on surface roughness and flank wear in hard-machining of DIN 1.2738 mold steel. *Sens. Rev.* **2019**, *39*, 24–33. [CrossRef]
33. Bousnina, K.; Hamza, A.; Ben Yahia, N. Predictive optimization of surface quality, cost, and energy consumption during milling alloy 2017A: An approach integrating GA-ANN and RSM models. *Int. J. Interact. Des. Manuf.* **2024**, *18*, 5177–5196. [CrossRef]
34. Küçük, Ö.; Kocakerim, M.M. Dissolution of ulexite-containing clay minerals in sulfur dioxide-saturated water. *Ind. Eng. Chem. Res.* **2005**, *44*, 1728–1733. [CrossRef]
35. Gao, Y.; Mi, S.; Zheng, H.; Wang, Q.; Wei, Z. An energy efficiency tool path optimization method using a discrete energy consumption path model. *Machines* **2022**, *10*, 348. [CrossRef]
36. Siddique, M.Z.; Faraz, M.I.; Butt, S.I.; Khan, R.; Petru, J.; Jaffery, S.H.I.; Khan, M.A.; Tahir, A.M. Parametric analysis of tool wear, surface roughness and energy consumption during turning of Inconel 718 under dry, wet and MQL conditions. *Machines* **2023**, *11*, 1008. [CrossRef]